Changing the Charge Distribution of β-Helical-Based Nanostructures Can Provide the Conditions for Charge Transfer

Nurit Haspel,* David Zanuy,† Jie Zheng,‡ Carlos Aleman,† Haim Wolfson,* and Ruth Nussinov‡§

*School of Computer Science Faculty of Exact Sciences, Tel Aviv University, Tel Aviv 69978, Israel; †Department of Chemical Engineering Escola Técnica Superior d'Enginyeria Industrial de Barcelona-Universitat Politécnica de Catalunya, 08028 Barcelona, Spain; ‡Basic Research Program Science Applications International Corporation-Frederick, Center for Cancer Research Nanobiology Program National Cancer Institute, NCI-Frederick, Frederick, Maryland 21702; and §Sackler Institute of Molecular Medicine, Department of Human Genetics, Sackler Faculty of Medicine, Tel Aviv University, Tel Aviv 69978, Israel

ABSTRACT In this work we present a computational approach to the design of nanostructures made of structural motifs taken from left-handed β-helical proteins. Previously, we suggested a structural model based on the self-assembly of motifs taken from *Escherichia coli* galactoside acetyltransferase (Protein Data Bank 1krr, chain A, residues 131–165, denoted krr1), which produced a very stable nanotube in molecular dynamics simulations. Here we modify this model by changing the charge distribution in the inner core of the system and testing the effect of this change on the structural arrangement of the construct. Our results demonstrate that it is possible to generate the proper conditions for charge transfer inside nanotubes based on assemblies of krr1 segment. The electronic transfer would be achieved by introducing different histidine ionization states in selected positions of the internal core of the construct, in addition to specific mutations with charged amino acids that altogether will allow the formation of coherent networks of aromatic ring stacking, salt-bridges, and hydrogen bonds.

INTRODUCTION

Nanotechnology aims to design novel materials and molecular devices, often via self-assembly of large molecules. In nature, protein domains often self-assemble and create large complexes of well-defined structure and function. Exploiting the natural ability of protein molecules to self-assemble can be a very useful approach in the design and construction of novel molecular structures (1–2). Many studies describe the use of natural and artificial peptides and DNA and RNA segments in nanodesign (3–11). Self-assembly of peptide segments can become a favorable route to obtain nanostructures, particularly those consisting of single or associated tubes, fibers, and vesicles. Binding mechanisms in self-assembly are robust and governed primarily by the protein's native topology (12).

Previously we suggested (13) that it is possible to construct nanostructures based on relatively large (~35 amino acid long) motifs taken from naturally occurring proteins. Specifically, we focused on structures made of the assembly of segments taken from left-handed β-helical proteins. The tubular nature of left-handed β-helical proteins makes them excellent candidates to be used as building blocks to construct fibrillar or tubular nanostructures without the need to perform many structural manipulations. In addition, their helical and symmetric structure makes them good candidates to be excised and tested as modules. To construct our nanosystems, we selected short (two turns) repetitive motifs and extracted the corresponding coordinates from the Protein Data Bank (PDB) (14). We assembled copies of the motifs on top of one another and simulated them for long periods. Of the systems we tested, the construct based on the assembly of copies of residues 131–165 of galactoside acetyltransferase from *Escherichia coli* (PDB code: 1krr, chain A) showed a remarkable structural stability over a long period of simulation time (20–40 ns) under all the tested temperature and ionic strength conditions. The system was denoted krr1. Fig. 1 shows the krr1 sequence and structure.

In this study we start with the krr1 structure we obtained previously (13) and aim to modify it toward useful biological functions. This construct is characterized by an internal hydrophobic core containing mainly valine and isoleucine residues, rendering it inappropriate for the transfer of matter or charge. Since the hollow space inside the structure we obtained is narrow and unsuitable for the transfer of large molecules, charge transfer seems to be one natural application. However, to allow charge transfer the chemistry of the internal core of the structure should be modified. Charge can be transferred through π-electron stacking or through H^+ transfer. We cannot directly simulate charge transfer through classical mechanics, but we can assess whether there are sufficient conditions to potentially allow it. We can either create ladders of π-electron-rich functional groups by substituting some of the original residues in the interior of the construct by other residues capable of π-stacking or generate a proton transfer environment through a network of salt bridges, reminiscent of the serine protease catalytic triad. The two necessary conditions to achieve this goal are

Submitted November 15, 2006, and accepted for publication February 23, 2007.

Address reprint requests to David Zanuy, Dept. of Chemical Engineering, ETSEIB-UPC, Diagonal 647, 08028 Barcelona, Spain. Tel.: 34-93-405-4447; Fax: 34-93-401-7150; E-mail: david.zanuy@upc.edu; or Ruth Nussinov, Center Cancer Research Nanobiology Program, NCI-Frederick, Bldg. 469, Rm. 151, Frederick, MD 21702. Tel.: 301-846-5579; Fax: 301-846-5598; E-mail: ruthn@ncifcrf.gov.

Editor: Robert Callender.

0006-3495/07/07/245/09 $2.00

doi: 10.1529/biophysj.106.100644

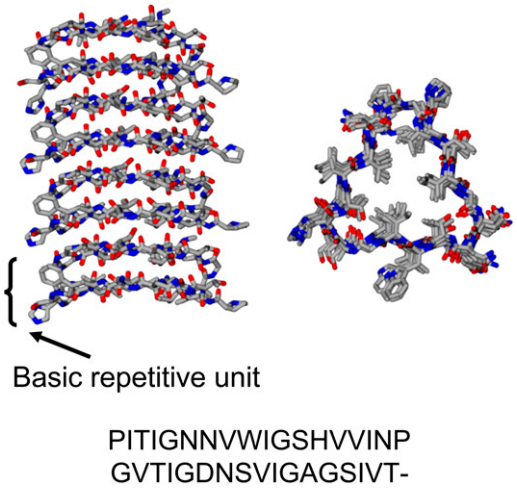

FIGURE 1 Sequence and structure of the construct made of residues 131–165 of *E. coli* galactoside acetyltransferase (PDB 1krr). On the left – a side view. Right – front view. Bottom – sequence alignment.

1. The mutated structures must still retain their tubular structural organization in the simulation.
2. There must be a side-chain distribution that allows the chemical processes mentioned above.

To create a ladder of π-stacking residues and to test whether this would affect the structural organization, we inserted a row of histidine residues in each of the three β-sheets, one sheet at a time (see Fig. 2 for an illustration of the three basic histidine mutants) and simulated the mutated structures. Histidine is a good choice of an amino acid for this purpose. It is aromatic and therefore capable of π-electron stacking. Its side chain resembles, more or less, the size of valine and isoleucine so we can expect that no drastic steric hindrance should occur. In addition, its pK_a is 6, which means that in a physiological pH it can assume both a neutral and a charged form with a relatively high probability. Moreover, its neutral form is actually equilibrium between two states: one with δ hydrogen (ND) protonated and the other with ε hydrogen (NE) protonated. This allows us to test different possible combinations of ionization states. Naturally, we could not sample all the possible ionization states due to computational time limitations, but we tried to sample as many possible positions as feasible to insert the histidines, as well as different combinations of ionization states. We identified a position where despite the insertion of histidine the simulated system retained its initial organization to a reasonable extent and created a configuration made of networks of neutral histidine, charged histidine, and aspartate, imitating the serine protease catalytic triad. We suggest a structure with a row of alternatively neutral and charged histidine residues that interact with a row of aspartate residues through salt bridges and with each other through aromatic ring stacking and thus provide the conditions for creating a nanosystem capable of charge transfer.

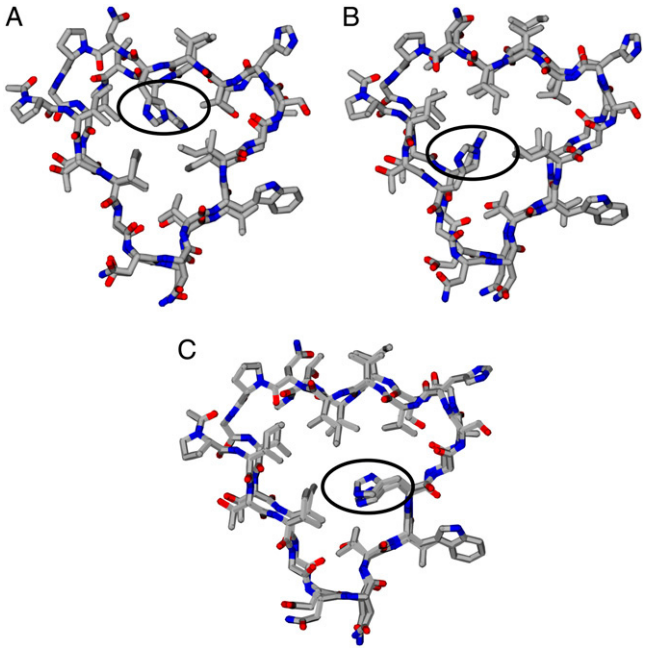

FIGURE 2 The basic units of krr1 with inserted histidine. Each of the three subfigures depicts a different position in which the histidine was inserted. (*A*) The histidine substitutes residues I-146 and V-164 (denoted krr_his1). (*B*) The histidine substitutes residues I-140 and I-158 (denoted krr_his2). (*C*) The histidine substitutes residues 134 and 152 (denoted krr_his3).

METHODS

The calculations were performed using the NAMD package (15). All the atoms of the system were considered explicitly, and the energy was calculated using the CHARMM22 force field (16). Water molecules were represented explicitly, using the TIP3 model (17). The simulations were performed using the NVT ensemble in an orthorhombic simulation box. We chose constant volume simulations because all the trajectories were obtained at high temperature. By these means we could assure not losing a proper density distribution due to thermal effects. Periodic boundary conditions were applied using the nearest image convention. The box size was adjusted to fit the complex size, so that infinite dilution conditions would be maintained. The box dimensions were $50 \times 50 \times 70$ Å to ensure infinite dilution. Some systems were simulated in a bounding box of size $60 \times 60 \times 80$ Å. Each system contained ~15,000–20,000 atoms including the solvent (or 27,000–30,000 in the structures with the larger bounding box). The starting molecular structures were built using the INSIGHTII molecular package (2000, Accelrys, San Diego, CA). For any given arrangement we fixed the interturn distance of adjacent repetitive units to match the interstrand distance within each unit, which was ~4.5 Å. The charge of all potential titratable groups was fixed at these values corresponding to neutral pH, such that all aspartic acid side chains were represented in their anionic form and all lysine side chains in their acidic positively charged form. Both peptide edges were capped to avoid interactions between adjacent termini.

We performed the simulations with ionic strength of 0.8% w/w (~24 ions) at 300° K. We kept the overall charge of the system neutral for the use of particle mesh Ewald summation (18) to calculate the electrostatic charges. The ions were chloride and sodium. The molecular dynamics protocol we used here has been used in our research group for some years (13,19–23) and has been proven to correspond to the experimental results (22,24–26). Before running each molecular dynamics simulation, the potential energy of each system was minimized using 5000 conjugate gradient steps. The heating protocol included 15 ps of increasing the temperature of the system from 0° to the final temperature of 300° K plus 1 ns of equilibration period.

A residue-based cutoff was applied at 14 Å, i.e., if any two molecules had any atoms within 14 Å, the interaction between them was evaluated. A numerical integration time step of 1 fs was used for all the simulations. The nonbonded pair list was updated every 20 steps, and the trajectories were saved every 1000 steps (1 ps) for subsequent analysis. Each simulation was run for a period of 20 ns.

Structural analysis

Regarding conservation of the size of the structure with respect to the minimized structure, the trajectories were aligned with the initial structure and the root mean-square deviation (RMSD) was calculated with respect to C-α atoms. The trajectories were sampled every 10 ps. The main-chain dihedral angles were sampled every 20 ps to maintain a good sampling of the trajectories but avoid a dense plot. The plots were generated with MATLAB. The figures were generated using MATLAB, VMD (27), and Rasmol (28).

RESULTS AND DISCUSSION

System description

The systems we constructed and simulated consisted of four repeats of a basic two-turn unit, containing altogether eight strand-loop motifs stacked on one another. Each basic repetitive unit was based on the PDB file of Galactoside acetyltransferase from *E. coli* (PDB code: 1krr, chain A, residues 131–165) and was represented at the atomic level.

Overall, we had nine histidine mutants, each with a different combination of protonation states (see Table 1). All systems were simulated in a water box for a period of 20 ns at 300° K. The simulations were performed using the NAMD program (15) (see Methods for a detailed description of the simulation conditions). To validate our results in an environment which is more reminiscent of physiological conditions, we added sodium and chloride ions to the solution and used the particle mesh Ewald summation (18) to evaluate the effect of ionic strength on the structural organization of our models. We used 24 ions, which leads to an ionic concentration of 0.8%, which is approximately the physiological concentration, keeping the overall charge of the system neutral to enable the Ewald summation. Fig. 3 shows the evolution of the RMSD with respect to the initial (minimized) structure of all the histidine-based simulated systems over time. We considered only the Cα atoms in the RMSD calculation, since side-chain atoms are flexible and calculating the evolution of their RMSD may introduce noise into the measurement.

For reference, we repeated the simulation of the wild-type krr1 under the same conditions and plotted the result in Fig. 3 *A*. As seen in the figure, some of the systems lasted well and kept their structural organization throughout the simulation, whereas other systems lost their structural organization to a considerable extent. The most stable system we obtained was when residues I-146 and V-164 (placed on top of one another in consecutive turns) were replaced by a neutral histidine with ND or NE protonated (denoted hsd1/hse1 mutants, respectively). Other structures were also able to maintain their structural arrangement to a degree, after the insertion of histidine (see the RMSD analysis in Fig. 3 and the structures before and after the simulations in Fig. 4). Since the neutral state in which the ND is protonated is more common in nature, we selected the hsd1 mutant as a reference structure for further simulations, as described below.

TABLE 1 The names and sequences of the krr1 histidine mutants

Name of mutant	sequence	Replaced residues
krr_hsd1	PITIGNNVWIGSHVV**H**NP	I-146→HSD
	GVTIGDNSVIGAGSI**H**T-	V-164→HSD
krr_hse1		I-146→HSE
		V-164→HSE
krr_his_alt1		I-146→HSD
		V-164→HSE
krr_hsd2	PITIGNNVW**H**GSHVVINP	I-140→HSD
	GVTIGDNSV**H**GAGSIVT-	I-158→HSD
krr_hse2		I-140→HSE
		I-158→HSE
krr_his_alt2		I-140→HSD
		I-158→HSE
krr_hsd3	PIT**H**GNNVWIGSHVVINP	I-134→HSD
	GVT**H**GDNSVIGAGSIVT-	I-152→HSD
krr_hse3		I-134→HSE
		I-152→HSE
krr_his_alt3		I-134→HSD
		I-152→HSE
krr_triad1*	PITIGNNVWIGSHVV**H**NP	I-146(1,3) →HSD
	GVTIGDNSVIGAGSI**D**T-	I-164(1,3) →ASP
	PITIGNNVWIGSHVV**H**NP	I-146(2,4) →HSP
	GVTIGDNSVIGAGSI**H**T-	I-164(2,4) →HSD
krr_triad2*	PITIGNNVWIGSHVV**H**NP	I-146(1,3,4) →HSD
	GVTIGDNSVIGAGSI**H**T-	I-164(1,3,4) →HSD
	PITIGNNVWIGSHVV**D**NP	I-146(2) →ASP
	GVTIGDNSVIGAGSI**H**T-	I-164(2) →HSP
krr_triad3	PITIGNNVWIGSH**D**V**H**NP	V-144→ASP
	GVTIGDNSVIGAGSI**H**T-	I-146→HSP
		I-164→HSD

HSD – neutral histidine with ND protonated; HSE – neutral histidine with NE protonated; HSP – positively charged histidine (both ND and NE protonated).
In some of the triad mutants, the sequence of two repetitive units is shown since in these mutants their sequences are different.
*The numbers in brackets in the right-hand column indicate the repetitive unit number. See Fig. 5.

The "serine triad"-like configuration

The concept that residues such as histidine can be placed inside a nanostructure brings to mind the possibility of using the nanostructures we designed as electron transfer devices (S. Kent, University of Chicago, personal communication, 2005). Histidines on consecutive strands are capable of stacking on one another, and the overlap between their π-electrons can potentially be used—along with a set of charged residues to supply the charge—for electron transfer.

We thus further modified the krr_hsd1 mutant, which is shown above to be structurally stable. We created a triad of amino acids, following the serine protease catalytic triad proton transfer system common in nature. As is well known,

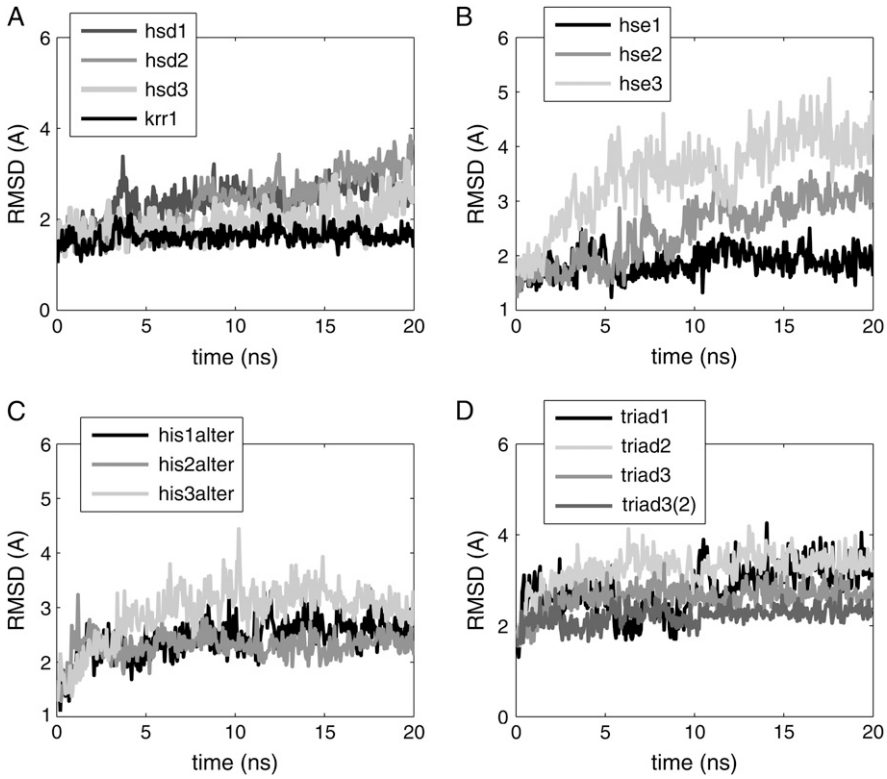

FIGURE 3 RMSD plot of the histidine mutants. The plot was divided into four panels for convenience: (*A*) neutral histidine, ND protonated; (*B*) neutral histidine, NE protonated; (*C*) neutral histidine, ND and NE protonated alternatively; and (*D*) his-asp-his+ triad containing systems. The system denoted triad3 was simulated twice for verification. The 1,2,3 annotations in panels *A–C* indicate mutants a, b, and c, respectively, as seen in Fig. 2. The wild-type krr1 is presented in (*A*) for reference.

this triad contains a Ser-His-Asp motif and a proton is transferred via the histidine changing its ionization state, with the serine being the hydrogen donor. Our triad was slightly different, using a neutral histidine instead of the serine to be the hydrogen-bond acceptor. Fig. 5 shows the structures of the histidine-aspartate triads.

We simulated three triad-containing structures for a period of 20 ns each (see Methods). The triad mutants differ from one another in the number of triads and their position in the structure. Fig. 5 shows the triad-containing structures. Fig. 3 *D* presents the RMSD of the triad systems throughout the simulations. The RMSD was measured with respect to the minimized structures, and only the Cα atoms were considered. As can be seen, all three triad structures got to within ~2.5–3 Å from the original structures. The construct denoted triad3 (whose structure is shown in detail in Fig. 5 *C*) is the most stable. Its structure adapts its conformation slightly in the first few nanoseconds of the simulations and later remains stable, and its RMSD hardly changes at all throughout the rest of the simulation. In this structure we inserted a row of alternatively neutral and charged histidine residues substituting residues Ile-146 and Val-164. Another row of aspartate residues replaced nearby residue Val-144. As can be seen in Fig. 5 *C*, the aspartate residues interact with the charged histidines, creating a network of salt bridges, whereas the neutral histidines take up the remaining space, avoiding a steric clash. The other triad structures did not fall apart either, but their terminal repetitive units started to fray, which indicates that given more time they would probably fall apart completely. To find out which parts of the structure fluctuated more than others during the simulation, we also analyzed the backbone conformational changes during the simulation.

Fig. 6 shows the distribution of the main-chain dihedral angles of the loop residues in the triad3 mutant. For comparison, Fig. 7 shows the distribution of the main-chain dihedral angles of the same residues in the krr1 wild-type. As mentioned above, residue 144 was mutated to Asp in triad3 and as can be seen in Fig. 6, *C* and *D*, the loop containing residues 141–144 and 159–162 fluctuated more than the other two loops (shown in Fig. 6, *A*, *B*, and *D*), as its residues explored a wider range of the conformational space. Moreover, that loop is considerably less stable in the triad3 mutant than the equivalent loop in the krr1 wild-type (shown in Fig. 7, *C* and *D*). However, residues 146 and 164, which were mutated to histidine in the triad3 system and are located on the adjacent β-sheet, did not fluctuate much (results not shown). Despite this, the triad3 structure was still able to maintain its overall organization. This can be rationalized by the following: The mutated loop had to readapt its structure since it was subject to additional conformational restrictions imposed by the salt bridges formed by the interaction between the Asp-144 side chain and the nearby charged histidine side chain (see Fig. 5). However, as seen in Fig. 6 *C*, it was Gly-141, which was located at the other end of the loop, that fluctuated the most during the simulation and explored the widest range of dihedral angles, whereas Asp-144 remained within a narrower range of side-chain conformations. This is

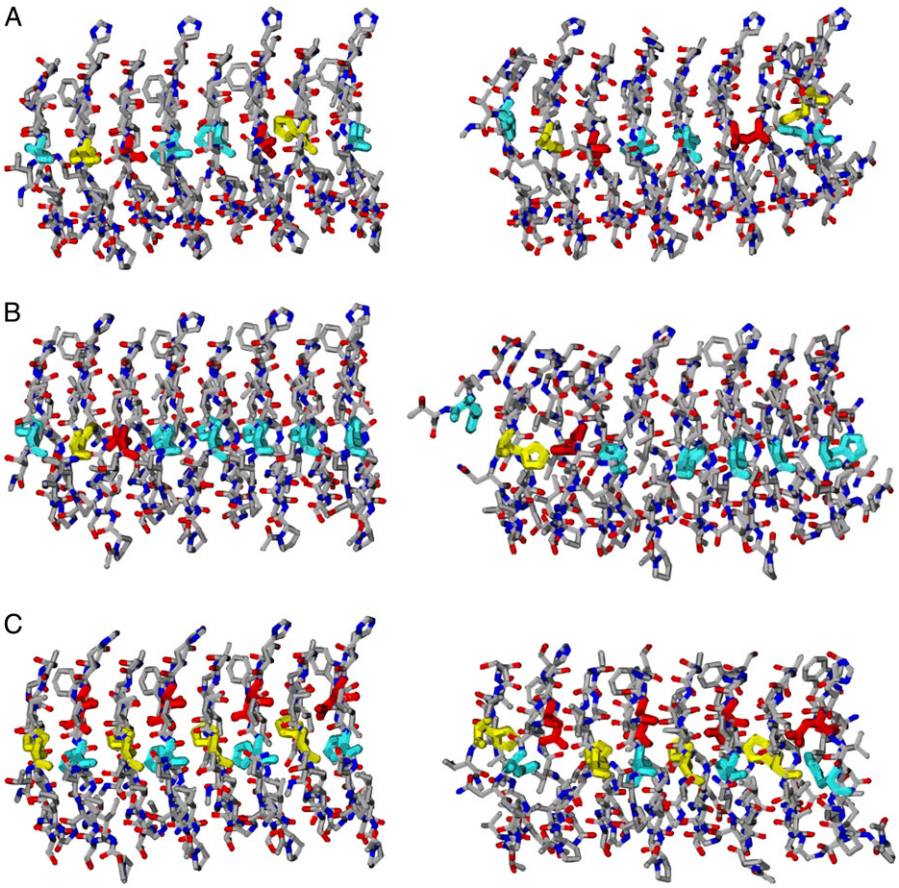

FIGURE 4 The three triad-containing systems before (*left*) and after (*right*) the simulation. (*A*) krr_triad1, (*B*) krr_triad2, (*C*) krr_triad3. The histidine residues are emphasized for clarity: neutral histidine is depicted in cyan, and charged histidine is depicted in yellow. The aspartate residues taking part in the triad are depicted in red. See Fig. 5 for a detailed description of the triads.

expected, since Asp-144 was restricted by the salt bridges with the nearby histidine side chain. We assume that due to the flexibility of the glycine, it absorbed most of the extra conformational restrictions and therefore helped keep the overall organization of the structure largely intact.

Interaction analysis

The histidine mutants are characterized by stacking interactions between the aromatic rings of histidine residues on equivalent positions on consecutive strands in the interior core of the structure. In addition, the triad3 mutant is characterized

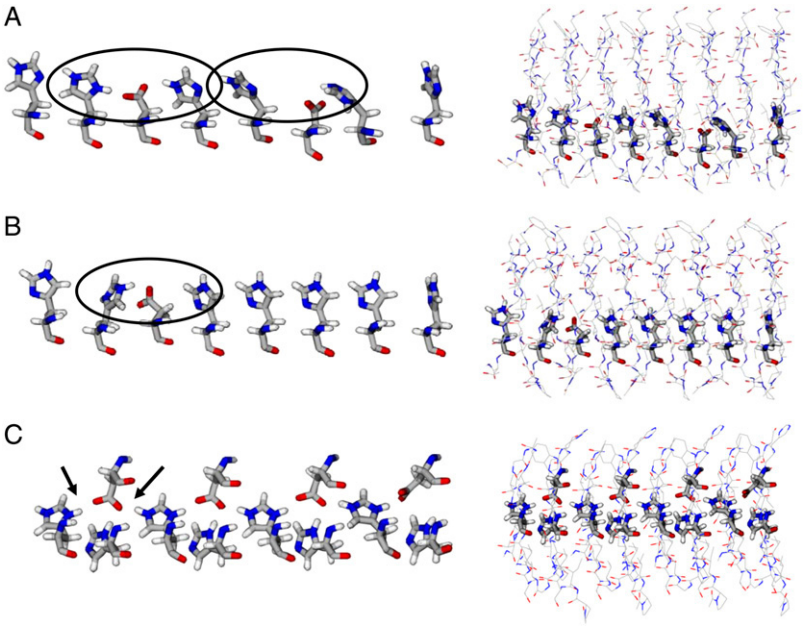

FIGURE 5 Three examples of the triad-containing structures: (*A*) triad1, (*B*) triad2, (*C*) triad3. In all cases on the left: only the triad. On the right: the entire system with the triad-containing row emphasized. The triad in *A* and *B* is emphasized and circled in black on the left. The salt bridge interactions are indicated by arrows in *C*.

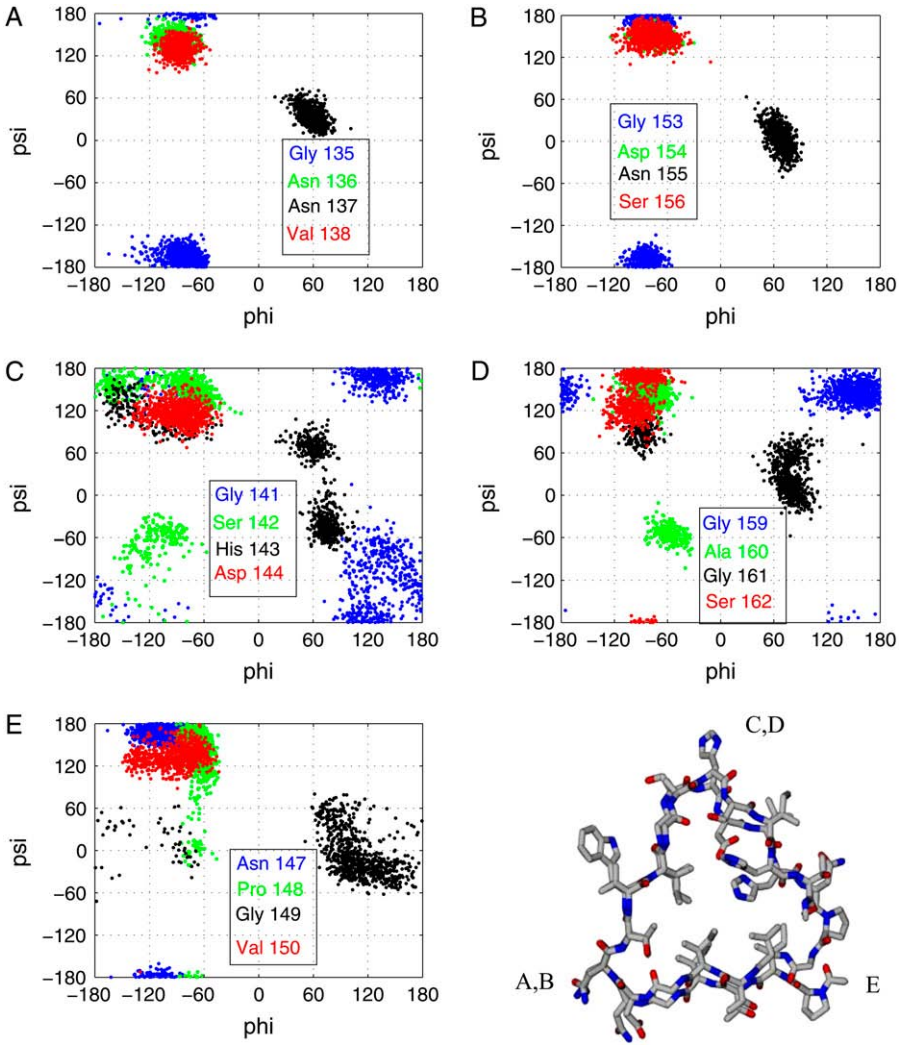

FIGURE 6 The main-chain dihedral angle distribution of the loop residues of the krr_triad3 mutant. For loop assignment, see bottom right illustration.

by a network of salt bridges between the negatively charged side chain of Asp-144 and the positively charged Hsp-164 (see an illustration of these interactions in Fig. 5 *C*). Table 2 summarizes the average salt-bridge distance between the Cγ of Asp-144 and the positively charged nitrogen atoms of Hsp-164 for both simulations of triad3. We considered an interaction as a salt bridge if the distance between the Asp Cγ atom and any of the Hsp-charged hydrogen atoms was $\leq$3.0 Å. We considered the distance to the Cγ atom instead of to the charged oxygen atoms of Asp (Oδ1 and Oδ2), since side-chain conformational changes during the simulation often cause the two oxygen atoms to flip. Therefore, measuring the distance of the Cγ from the positively charged histidine hydrogen is more robust and provides a good estimate as to the location of the Oδ1 and Oδ2 atoms with respect to the His positively charged group.

As seen in the table, the average distance of interaction for the salt bridges is $\sim$2.7 Å in both simulations, which indicates a strong electrostatic attraction, since the charged Asp oxygen atoms are even closer to the Hsp hydrogens than the Asp Cγ. It is also seen that nearly all seven possible interactions existed at any given trajectory during the simulation and that the standard deviation of the measured distance was small ($\sim\pm$0.2 Å), indicating that the distances were rather restrained and did not change much during the simulation, in accordance with the fact that the structure in general maintained its organization. Table 2 also shows the average distance and angle of the aromatic ring stacking between consecutive histidine residues in both the triad3 mutants and the hsd1 mutant, whose basic repetitive unit is shown in Fig. 2 *A*. We considered a maximum distance of 7.0 Å between the centers of masses of the measured rings. As seen in the table, the average stacking distance is 4.9–5.2 Å. In addition, all seven possible stacking interactions existed in nearly all the simulations, especially in the two triad3 simulations. The standard deviations were also rather small, considerably less than 1.0 Å in all cases, indicating that the distances between consecutive histidine rings did not fluctuate much during the simulation, again in accordance with the overall good organization of the structures.

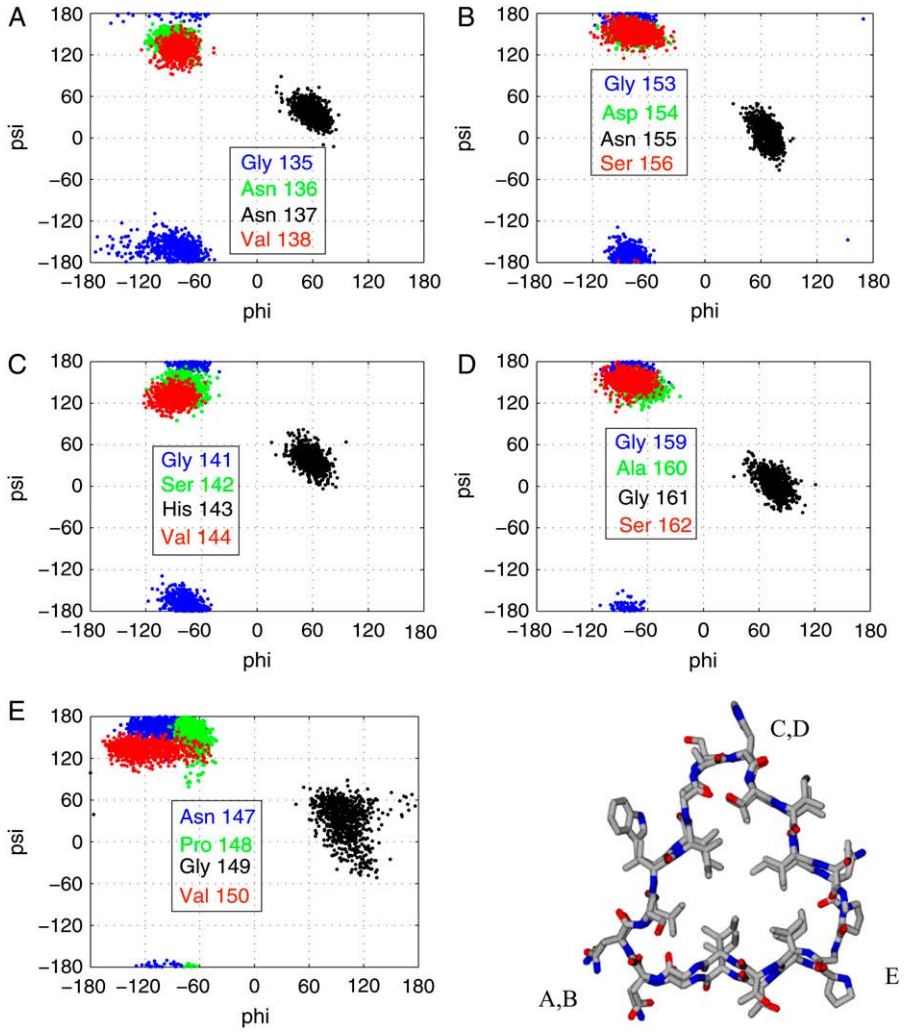

FIGURE 7 The main-chain dihedral angle distribution of the loop residues of the wild-type krr1, when simulated with 24 ions (0.8% w/w). For loop assignment, see bottom right illustration.

Looking at the average angle between consecutive aromatic rings, also shown in the table, one can see that not surprisingly in the hsd1 mutant the aromatic ring's stacking was significantly more parallel than in the triad3 mutants, where the stacking tended to be T-shaped. In the triad3 mutants the positively charged histidine rings adapted their conformation to interact with the Asp-144 oxygens and created the energetically preferred electrostatic interactions. The remaining neutral histidine rings could not align with the charged rings, as this would cause a steric clash with the Asp residues (see Fig. 5 *C*) and therefore the stacking angles were closer to 90°. Despite the fact that T-shaped stacking is weaker than parallel stacking, it is still strong enough to potentially enable a partial overlap of the π-electrons of the rings. To prove that T-shaped stacking is a consequence of the nanoconstruct organization more than the effect of adding to stacking the electrostatic component (Asp^{-}-His^{+} pairs), we performed quantum mechanical calculations using molecular models that mimic the triad organization. Results indicated that T-shape stacking is disfavored with respect to classical face to face stacking, even when electrostatic interactions are involved. Therefore, the steric restrictions imposed by the nanostructure organization are responsible for the formation of a T-shaped arrangement since they are energetically less

TABLE 2 Average distance of salt bridges and aromatic ring stacking in the relevant histidine mutants

Mutant name	Average salt bridge (Å)	Average number of salt bridges*	Average aromatic ring distance (Å)	Average aromatic ring angle (degrees)	Average number of ring stacking*
krr_hsd1	N/A	N/A	4.944 ± 0.47	28.12 ± 14.56	5.997
krr_triad3 (I)	2.72 ± 0.14	6.62	5.20 ± 0.89	71.01 ± 23.97	6.75
krr_triad3 (II)	2.70 ± 0.2	6.07	5.19 ± 0.68	63.37 ± 18.04	6.59

*Out of seven possible interactions.

favored (results are shown in the Supplementary Material). The overall scenario drawn by our results demonstrates a potential use of the krr1-based models to transfer charge.

CONCLUSIONS

We have shown before that β-helical proteins are promising candidates for nanostructure design for several reasons: They are repetitive, tubular, and symmetrical and thus suitable for designing new nanomaterials of a repetitive nature such as nanofibers and tubes. In addition, their tube-like structure makes them of potential use for targeted small molecule delivery, fiber construction with attached imaging probes, or targeted peptides and charge transfer. We were able to show that a system constructed of four replicas of residues 131–165 of galactoside acetyltransferase exhibited remarkable stability under all the simulated conditions, including temperature increase and addition of ions. In this work we take our findings one step further and show that we can modify the original sequence of our construct and substitute specific residues in the internal core by histidine while maintaining the original structure throughout the simulation time. This, in turn, shows that it is possible to modify the residue composition and the hydrophobicity of the interior core of a β-helical-based construct and still maintain structural organization. We also inserted a row of aspartate residues in a position that enabled the creation of a network of salt bridges and hydrogen bonds with the histidine side chains, following the serine protease catalytic triad seen in nature, while largely maintaining the original structural organization. This suggests that there is potential use of these systems for charge transfer. This hypothesis requires further testing and experimenting. Further research directions may include more extensive simulations, including the introduction of point mutations to standard and nonstandard amino acids to enhance the structural stability of the systems. Another direction of future study could be to perform more quantum mechanical calculations to test the hypothesis that the triad-containing constructs are suitable for charge transfer. Another direction would be to experimentally produce the constructs and test their structural stability in vitro.

SUPPLEMENTARY MATERIAL

An online supplement to this article can be found by visiting BJ Online at http://www.biophysj.org.

We thank Steve Kent who, during his visit to the NCI-Frederick in the summer of 2005, suggested the usage of the self-assembled β-helices' repeats for electron transfer. Computation times are provided by the National Cancer Institute's Frederick Advanced Biomedical Supercomputing Center and by the NIH Biowulf.

This project has been funded in whole or in part with federal funds from the National Cancer Institute, National Institutes of Health (NIH), under contract number NO1-CO12400. The content of this publication does not necessarily reflect the view or policies of the Department of Health and Human Services, nor does mention of trade names, commercial products, or organization imply endorsement by the U.S. government. This research was supported (in part) by the Intramural Research Program of the NIH, National Cancer Institute, Center for Cancer Research. Part of the computer resources was generously provided by the Barcelona Supercomputer Center (BSC).

REFERENCES

1. Zhang, S., D. M. Marini, W. Hwang, and S. Sansoto. 2002. Design of nanostructured biological materials through self-assembly of peptides and proteins. *Curr. Opin. Chem. Biol.* 6:865–871.
2. Zhang, S. 2003. Fabrication of novel biomaterials through molecular self assembly (review). *Nat. Biotechnol.* 21:1171–1178.
3. Rajagopal, K., and J. P. Schneider. 2004. Self-assembling peptides and proteins for nanotechnological applications (review). *Curr. Opin. Struct. Biol.* 14:480–486.
4. Claussen, R. C., B. M. Rabatic, and S. I. Stupp. 2003. Aqueous self-assembly of unsymmetric peptide bolaamphiphiles into nanofibers with hydrophilic cores and surfaces. *J. Am. Chem. Soc.* 125:12680–12681.
5. Percec, V., A. E. Dulcey, V. S. Balagurusamy, Y. Miura, J. Smidrkal, M. Peterca, S. Nummelin, U. Edlund, S. D. Hudson, P. A. Heiney, H. Duan, S. N. Magonov, and S. A. Vinogradov. 2004. Self-assembly of amphiphilic dendritic dipeptides into helical pores. *Nature.* 430: 764–768.
6. Reches, M., and E. Gazit. 2003. Casting metal nanowires within discrete self-assembled peptide nanotubes. *Science.* 300:625–627.
7. Matsuura, K., K. Murasato, and N. Kimizuka. 2005. Artificial peptide-nanospheres self-assembled from three-way junctions of beta sheet forming peptides. *J. Am. Chem. Soc.* 127:10148–10149.
8. Holowka, E., D. J. Pochan, and T. J. Deming. 2005. Charged polypeptide vesicles with controllable diameter. *J. Am. Chem. Soc.* 127:12423–12428.
9. Hall, C. K., and V. A. Wagoner. 2006. Computational approaches to fibril structure and formation. *Methods Enzymol.* 412:338–365.
10. Iengar, P., N. V. Joshi, and P. Balaram. 2006. Conformational and sequence signatures in beta helix proteins. *Structure.* 14:529–542.
11. Elber, R. 2005. Long-timescale simulation methods. *Curr. Opin. Struct. Biol.* 15:151–156.
12. Levy, Y., and J. N. Onuchic. 2006. Mechanisms of protein assembly: lessons from minimalist models. *Acc. Chem. Res.* 39:135–142.
13. Haspel, N., D. Zanuy, C. Aleman, H. Wolfson, and R. Nussinov. 2006. De-novo tubular nanostructure design based on self-assembly of beta-helical protein motifs. *Structure.* 14:1137–1148.
14. Bernstein, F. C., T. F. Koetzle, G. J. B. Williams, E. F. Meyer, M. D. Brice, J. R. Rodgers, O. Kennard, T. Shimanouchi, and M. Tasumi. 1977. The *Protein* Data Bank: a computer-based archival file for macromolecular structures. *J. Mol. Biol.* 112:535–542.
15. Kale, L., R. Skeel, M. Bhandarkar, R. Brunner, A. Gursoy, N. Krawetz, J. Phillips, A. Shinozaki, K. Varadarajan, and K. Schulten. 1999. NAMD2: greater scalability for parallel molecular dynamics. *J. Comput. Phys.* 151:283–312.
16. MacKerell, J. A. D., D. Bashford, M. Bellott, R. L. J. Dunbrack, J. Evanseck, and M. J. Field. 1998. All-hydrogen empirical potential for molecular modeling and dynamic studies of proteins using the CHARMM22 force field. *J. Phys. Chem. B.* 102:3586–3616.
17. Jorgensen, W. L., J. Chandrasekhar, J. D. Madura, R. W. Impey, and M. L. Klein. 1982. Comparison of simple potential functions for simulating liquid water. *J. Chem. Phys.* 79:926–935.
18. Darden, T., D. York, and L. Pedersen. 1993. Particle mesh Ewald: an N*log(N) method for Ewald sums in large systems. *J. Chem. Phys.* 98:10089–10092.
19. Ma, B., and R. Nussinov. 2002. Stabilities and conformations of Alzheimer's beta-amyloid peptide oligomers (A-b16–22, A-b16–35, A-b10–35): sequence effects. *Proc. Natl. Acad. Sci. USA.* 99:14126–14131.

20. Zanuy, D., B. Ma, and R. Nussinov. 2003. Short peptide amyloid organization: stabilities and conformations of the islet amyloid peptide NFGAIL. *Biophys. J.* 84:1–11.

21. Zanuy, D., and R. Nussinov. 2003. The sequence dependence of fiber organization: a comparative molecular dynamics study of the islet amyloid polypeptide segments 22–27 and 22–29. *J. Mol. Biol.* 329:565–584.

22. Zanuy, D., Y. Porat, E. Gazit, and R. Nussinov. 2004. Peptide sequence and amyloid formation: molecular simulations and experimental study of a human islet amyloid polypeptide fragment and its analogs. *Structure.* 12:439–455.

23. Haspel, N., D. Zanuy, B. Ma, H. Wolfson, and R. Nussinov. 2005. A comparative study of amyloid fibril formation by residues 15–19 of the human calcitonin hormone: a single beta-sheet model with a small hydrophobic core. *J. Mol. Biol.* 345:1213–1227.

24. Petkova, A. T., Y. Ishii, J. J. Balbach, O. N. Antzutkin, R. D. Leapman, F. Delaglio, and R. Tycko. 2002. A structural model for Alzheimer's b-amyloid fibrils based on experimental constraints from solid state NMR. *Proc. Natl. Acad. Sci. USA.* 99:16742–16747.

25. Reches, M., Y. Porat, and E. Gazit. 2002. Amyloid fibril formation by pentapeptide and tetrapeptide fragments of human calcitonin. *J. Biol. Chem.* 277:35475–35480.

26. Luehrs, T., C. Ritter, M. Adrian, D. Riek-Loher, B. Bohrmann, H. Doebeli, D. Schubert, and R. Riek. 2005. 3D structure of Alzheimer's amyloid b-(1–42) fibrils. *Proc. Natl. Acad. Sci. USA.* 102:17342–17347.

27. Humphrey, W., A. Dalke, and K. Schulten. 1996. VMD: visual molecular dynamics. *J. Mol. Graph.* 14:33–38.

28. Sayle, R., and J. E. Milner-White. 1995. RasMol: biomolecular graphics for all. *Trends Biochem. Sci.* 20:374.